A Method to Quantify Technical-Economic Aspects of HTS Electric Power Cables

A method to quantify technical-economic aspects of HTS electric power cables

A. Musso, G. Angeli, M. Bocchi, P. L. Ribani and M. Breschi

Abstract — **In prevision of an expansion in the installed power and the progressive increase in electrification toward energy transition, high-efficiency electric grids are required. In this process, superconducting power cables could play an important role as they can be installed either to realize new lines or to replace existing infrastructures, potentially reducing the costs and the environmental impact compared to conventional solutions.**

The technical-economic convenience of the superconducting choice depends on the design parameters of the line, such as the voltage and power levels and the line length. For each condition, the configuration of the cable and its cooling system must be optimized while complying with a number of electrical and geometrical constraints. Identifying a priori the optimal cable configuration is not trivial, as the numerous variables involved are mutually dependent. This work provides a tool to quantify technical-economic aspects of superconducting cables, allowing the user to freely select the operating conditions for a generic electric line. The tool adopts a genetic algorithm to solve a constrained minimization problem for a multi-variable function, returning the cable configuration characterized by the lowest costs.

For this study, AC concentric cables realized with High Temperature Superconductors (HTS) are selected, but the approach described can easily be adapted to other types of cable. By means of suitable simplifying hypotheses, the equations used to size the cable components and their corresponding costs, estimate the thermal inputs and describe the cryogen flows are introduced as parametric equations. Finally, the results of a detailed study on the impact of the relevant parameters on the cable design and costs is provided.

Index Terms —**High Temperature Superconductors, Superconducting Cables, Concentric Cables, Optimization Methods, Costs.**

I. Introduction

The first detailed studies regarding the use of superconducting materials for manufacturing power cables, date back to the second half of the 1960s [1 – 2]. The prototypes were based on the use of Low Temperature Superconducting materials, cooled with liquid helium. These devices were highly expensive and required particularly complex and cumbersome cryogenic systems, necessary to cope with the losses generated under alternate current (AC) conditions. For these reasons, the application of superconducting cables to the transport of high power was initially limited to direct current (DC) regimes and in controlled environments, such as laboratories for high energy physics [3]. Then, the discovery of High Temperature Superconductors (HTS), to be used at liquid nitrogen temperature, renewed interest in the use of AC cables, allowing simpler and cheaper cryogenic systems.

Numerous prototypes have been developed since the early 2000s, using HTS cables in different configurations. The first distinction is between Warm Dielectric (WD) and Cold Dielectric (CD) cables [4]. In WD cables, the dielectric is located outside the cryostat, while in CD cables it is contained inside the cryostat, at the same temperature of the superconductor. Compared to WD cables, the CD configuration makes it easier to access the cryostat, as it is electrically insulated from the conductive phases. However, designing a CD cable is a complex task due to the number of components at cryogenic temperatures (terminations, joints, electrical insulation, etc.). Most superconducting cable prototypes proposed in the last years were designed using the CD configuration [5 – 17], while publications related to WD prototypes have significantly decreased over time [18 – 21].

Furthermore, different CD cable layouts have been proposed in the literature for AC power lines, mainly belonging to the following three categories. In *single-core cables*, each phase is contained in a different cryostat [22]. In *3-in-1 cables*, the three phases are included within the same cryostat, and their conductors are helically wound around three distinct axes. In *concentric cables* (also known as coaxial cables), the three phases are helically wound around the same axis, one on top of the other, separated by dielectric layers. Fig. 1 shows a sketch of the lateral view of this cable layout. The main advantage of concentric cables is that, if the three phases are perfectly balanced (uniform current distribution between tapes and phases), the magnetic field outside the phases is canceled out, without the need of a superconducting shield [3, 23]. This reduces the amount of superconductor needed compared to the other CD configurations, thereby significantly reducing cost and complexity. Moreover, the concentric configuration is compact and thus suited to be contained in the tunnels made for conventional lines, thus facilitating their retrofitting.

Once the various superconducting cable layouts have been defined, one should ask whether their use in the electric grid can be competitive compared to conventional cables, when, for example, it is necessary to replace an old line or to realize a new one.

A. Musso, M. Breschi and P. L. Ribani are with the Department of Electrical, Electronic and Information Engineering, of the University of Bologna, 40136 Bologna, Italy (e-mail: andrea.musso3@unibo.it).

G. Angeli and M. Bocchi are with RSE S.p.A., 20134 Milan, Italy.

Color versions of one or more of the figures in this paper are available online at http://ieeexplore.ieee.org.

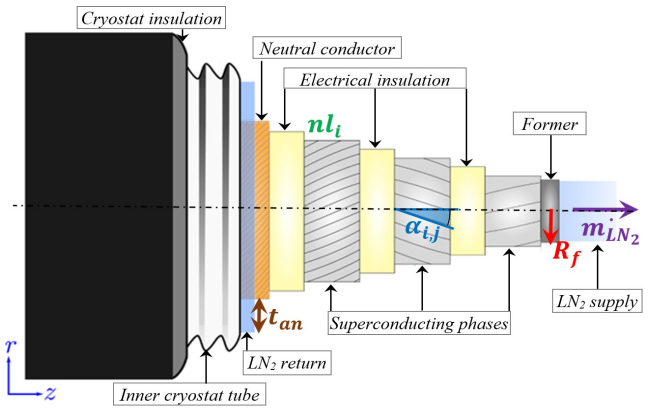

Fig. 1. Sketch of the lateral view of a concentric HTS cable highlighting some of the parameters selected as variables of the problem (bold coloured terms). The figure is not in scale [24].

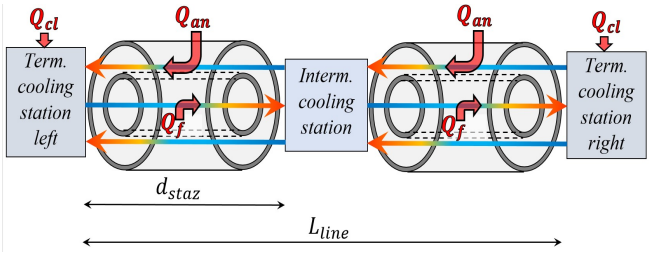

Fig. 2. Sketch of the both-sided cooling option with a single intermediate cooling station. The colored arrows represent the coolant heating up while flowing through the cable. The bold red terms indicate the heat inputs to the system and to the cooling stations.

To answer this question, the optimization of the cable design according to the operating conditions and a proper estimation of the cost of the whole superconducting system must be performed. A large industrial production of superconducting cables for the electric grid does not exist yet; thus, these data are not easily available in the literature and generally refer to specific case studies. The purpose of this work is to develop a tool to quantify technical-economic aspects of superconducting cables, allowing the user to freely select the operating conditions of interest for a generic electric line. The methodology presented allows one to determine the cable design for the selected conditions, optimized to reduce the cost of the entire system while complying with the physical and geometric constraints imposed by the problem.

To limit the otherwise too broad field of investigation, a specific superconducting cable configuration is selected for this analysis, which the authors consider as one of the most promising for future developments of this technology. This work focuses on CD concentric cables wound with coated conductors, cooled using liquid nitrogen, for the use in AC power lines at medium voltage levels in the electric grid (from 10 to 30 kV). However, the logical-mathematical approach proposed can be adapted to other types of cables.

In Chapter II, the main features of the optimization tool and the variables chosen for this study are reported. Chapter III reports the method for the calculation of the losses and the heat inputs in the system. Chapter IV describes the procedure for the computation of the thicknesses of the dielectric layers. Chapter V details the implementation of the physical constraints in the mathematical model. In Chapter VI, the cost function implemented in the algorithm is described. Chapter VII lists the user-defined input parameters adopted, with the corresponding references. Finally, the results of some relevant parametric analyses are shown in Chapter VIII, providing an interpretation on the impact of specific variables on the cable design and costs.

II. Description of the Tool Main Features

The algorithm developed allows one to determine the optimized cable design according to the operating parameters selected. Mathematically, a constrained minimization problem for a multi-variable function (the cost of the cable system) has to be solved. In this work, the genetic algorithm solver (*ga*) implemented in the MATLAB software [25] is adopted. The *ga* solver is selected as it easily allows one to impose some variables involved in the optimization to be integers. The solver returns the values of the set of variables corresponding to the lowest system cost. Since a genetic algorithm is a stochastic method, it can return slightly different solutions starting from the same initial conditions. Thus, the tool runs the code 5 times consecutively (a value set after a convergence analysis), finding a solution at each iteration; among these solutions, the one that leads to the lowest value of the cost function is selected. Then, the tool returns the cable design parameters corresponding to that solution.

A. Selection of the system variables

In the present study, the number of variables is limited to the parameters considered as more relevant for the cable design. This procedure allows one to identify their correlation with the cable cost while keeping the computational burden of the solver minimal. The remaining parameters are set or computed from the main variables; however, the user can modify their value to carry out specific parametric analyses.

Fig. 1 highlights some of the variables selected for the optimization (see the bold colored terms). R_f is the inner radius of the cable former, t_{an} the thickness of the annular gap, $\dot{m}_{LN2}$ the mass flow rate of the coolant, nl_i the number of superconducting layers of the i^{th} phase and $\alpha_{i,j}$ the winding angle of the tapes of the j^{th} layer of the i^{th} phase.

It is worth noting that the radial size of the cable depends on the parameters R_f, t_{an} and nl_i only. As described in Chapter IV, the thickness of each dielectric layer is imposed by the selected voltage level and by the radius of the underlying conductive phase. The thicknesses of the other layers (*e.g.* the former, the HTS tapes, the neutral conductor, the cryostat walls) are input parameters and their values can be modified by the user.

The last selected variable corresponds to the number of intermediate cooling stations along the cable (n_{stat}). They are distinguished from the termination cooling stations, which are located at the line ends. In this study, it is assumed that properly

sized termination stations have to be included in the system, regardless of the cable length L_{line}. In fact, among the different options of cable cooling configurations [26], the so-called *both-sided cooling option* is adopted. As shown in Fig. 2, this design includes a forward flow of coolant within the central former (the arrow from left to right), and a return flow through an annular gap between the neutral conductor and the inner cryostat tube (the arrows from right to left). This configuration does not require any external coolant return. Therefore, each station has to manage two coolant flows in opposite directions, and must be capable to restore their temperature and pressure to the initial conditions selected by the user. The calculation of the cooling power required for the termination and intermediate stations is reported in Chapter III. For sufficiently long lines, the presence of intermediate cooling stations could be necessary to ensure the coolant (*e.g.* liquid nitrogen) to remain in its subcooled liquid conditions along the whole cable length and that no boiling phenomena occur, that would affect the heat exchange efficiency. However, it may be economically convenient to introduce more cooling stations than the minimum required, so as to reduce the average temperature of all conductor components, and improve the transport properties of the coated conductors by increasing their critical current.

B. Thermal considerations

As shown in Fig. 2, the cable is modular and can be divided into segments included between two consequent cooling stations. Moreover, it is assumed that adjacent cooling stations are all placed at the same distance from each other ($d_{stat} = L_{line}/(n_{stat} - 1)$). This allows one keeping the same cable design for each cable segment; moreover, all the intermediate cooling stations can be equally sized. In fact, the intermediate cooling stations must manage two inlet cryogen counter-flows, each absorbing a specific amount of heat within a single segment. These heat inputs correspond to Q_f for the nitrogen flowing in the former and Q_{an} for the nitrogen flowing in the annular gap. Q_f and Q_{an} can differ from each other, but their values are assumed constant in each cable segment. Thus, assuming that $\dot{m}_{LN2}$ is the same in both flows, each intermediate cooling station must remove an equal amount of heat.

The termination cooling stations have to manage only one "warm" inlet flow of coolant. As shown in Fig. 2, the termination cooling station at the left side of the cable manages the heat coming from the nitrogen in the annular gap, while the one located at the right side of the cable manages the heat coming from the nitrogen flowing in the former. Moreover, they both have to handle the losses from the current leads (Q_{cl}). Since Q_f and Q_{an} can be distinct, the two termination cooling stations can be differently sized. It is worth noting that the directions of the two cryogen flows chosen in Fig. 2 are arbitrary (under the constraint to be opposite), and the definition of left and right ends is for descriptive purposes only.

Then, some assumptions have to be made on the operating temperature of the coated conductors, since it affects the tapes critical current (I_c) and thus the amount of superconducting material required to guarantee the cable transport properties while

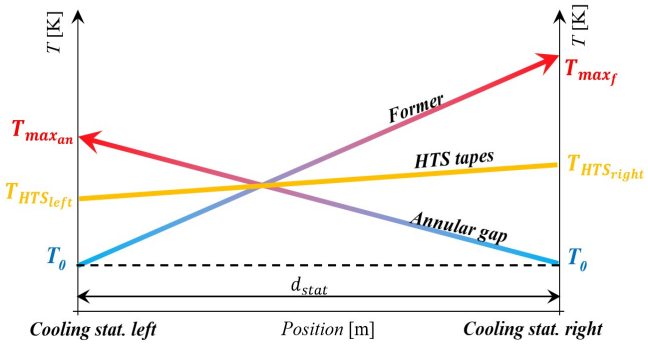

Fig. 3. Temperature trends in nitrogen flows and HTS tapes in a generic cable segment. The figure is not in scale.

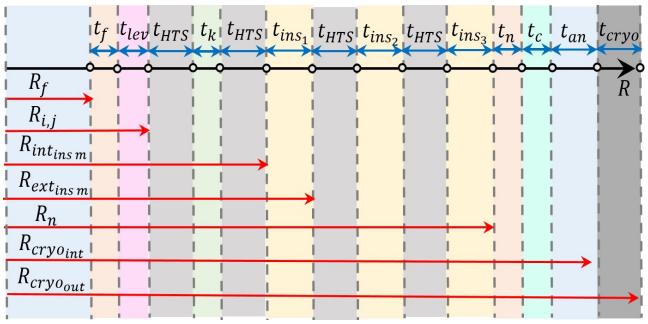

Fig. 4. Sketch of a symmetric portion of the cross-section of a centric cable with two HTS layers in phase 1 and one HTS layer in phases 2 and 3. The arrows highlight the geometric parameters along the radial direction of the cable, used in the tool. The figure is not in scale. The symbols are explained in the following text.

complying with the electrical constraints. The model presented here neglects the temperature distribution over the superconducting layers in the same cross-section, thus assuming a single temperature for all tapes at each longitudinal position. Since the tapes are included between the two cryogen flows, this temperature is computed as the average of the nitrogen temperatures in the two flows at the given location. It is assumed that both cryogen flows exit from a cooling station at the same temperature T_0 (in subcooled conditions) and they are subjected to given temperature rises up to the next station.

These temperature rises depend on the heat absorbed by each flow, Q_f and Q_{an}, and on the frictional losses in each pipe; their approximate analytic functions are described in Chapter V.D. Since these terms can be different, the maximum temperatures reached by the nitrogen in the former and in the annular gap in a cable segment, T_{max_f} and $T_{max_{an}}$ respectively, can also be different. Thus, following the scheme shown in Fig.3 and indicating with x the longitudinal coordinate of a cable segment of length d_{stat}, the temperature of the tapes (T_{HTS}) varies linearly between the following values:

$$T_{HTS}\,(x = 0) = T_{HTS_{left}} = \left(T_{max_{an}} + T_0\right)/2$$
$$T_{HTS}\,(x = d_{stat}) = T_{HTS_{right}} = \left(T_{max_f} + T_0\right)/2 \quad (1)$$

C. Geometrical considerations

Fig. 4 shows a diagram of one half of the cross-section of the concentric cable; the cable is symmetrical with respect to the radial direction. The figure presents the different geometric parameters introduced in the model. The colored areas indicate the different concentric layers; the red arrows at the bottom indicate the main radial parameters of the model, while the blue arrows at the top indicate the main thicknesses.

In particular, $R_{i,j}$ is the inner radius of the of the j^{th} HTS layer of the i^{th} phase, $R_{int_{ins\,w}}$ and $R_{ext_{ins\,w}}$ are the inner and outer radii of the m^{th} dielectric layer, respectively. R_n is the radius of the copper neutral conductor and $R_{cryo_{ext}}$ and $R_{cryo_{int}}$ are the outer and inner radii of the cryostat, respectively. t_f is the former thickness. t_{lev} is the thickness of the levelling layers wound around the former to protect the innermost superconducting layer against deformation [26]. t_{HTS} is the thickness of each superconducting tape and t_k is the thickness of the Kapton insulation interposed between the HTS layers of the same phase. t_{ins_m} is the thickness of the m^{th} dielectric layer. t_n is the copper neutral thickness and t_c is the former thickness of the cable core fixture interposed between the neutral conductor and the annular gap, added to give mechanical stabilization during the cable assembly and operations. Finally, t_{cryo} is the thickness of the cryostat walls.

III. Description of the Loss Function

An appropriate estimation of losses during the cable operation is required for the correct dimensioning of the refrigeration system, since it affects the temperature of the cryogenic fluid (and in cascade, all the parameters of the cable design). Calculation using finite element models can lead to a great level of accuracy, but would have a significant impact on the computational burden of the proposed model. Therefore, the use of fast-performing analytical formulae, herein described, is preferred.

The losses and the heat inputs produced or entering in a generic cable segment are absorbed by the nitrogen flowing into the former and the annular gap. This study assumes that the loss terms are shared equally between the two flows, with the exception of the heat entering the cryostat from outside, which is absorbed by the nitrogen in the annular gap only. Under these assumptions, the following equation holds:

$$\begin{aligned} Q_f(T_{max_f}, T_{max_{an}}) &= (Q_{AC} + Q_{ins} + Q_{ed})/2 \\ Q_{an}(T_{max_f}, T_{max_{an}}) &= Q_{cryo} + (Q_{AC} + Q_{ins} + Q_{ed})/2 \end{aligned} \tag{2}$$

where Q_{AC} are the AC losses in the superconducting tapes, Q_{ins} are the losses generated in the electric insulation, Q_{ed} are the eddy current losses in the normal conducting materials and Q_{cryo} is the heat input from the cryostat walls. These terms refer to the losses in a single cable segment of length d_{staz}.
In (2) the loss dependence of Q_f and Q_{an} on T_{max_f} and $T_{max_{an}}$ is highlighted. This is due to the term Q_{AC}, as illustrated in the next chapter.

As far as the losses generated in the current leads at the terminations (Q_{cl}) are concerned, they are generally reported as a function of the amplitude of the design current of the cable (q_{cl}), to be multiplied by the number of current leads required, based on the cable configuration selected [3]. In the case of a concentric cable (no superconducting shield), 3 current leads are needed at each cable ends.

A. AC losses

In the literature, several formulae have been presented for the calculation of hysteresis losses in the superconducting material of HTS cables, based on different assumptions. The main ones are the Norris' formulation [27], the monoblock [28] and duoblock [29] models, the formulation proposed by Clem and Malozemoff [30] and the "gap and polygonal" loss model [31]. The results obtained using different formulae can differ significantly; thus the choice of the model affects the cable design. In this paper, the Norris' formulation is adopted and applied to the geometry of a coaxial cable. This is a precautionary choice, since generally Norris' model provides an upper limit to the estimate value of losses, compared to other approaches [24, 32, 33]. The authors plan to dedicate future analyses to the choice of different methodologies for estimating AC losses to implement in the proposed tool.

In this work, Q_{AC} is the sum of the losses generated in the single tapes of the cable, approximated as straight independent conductors. Since T_{HTS} varies along the longitudinal coordinate of a cable segment x, so does I_c and the HTS AC losses. For this reason, an integral of the losses per unit length is carried out for each layer, over the total tape length included in a cable segment ($L_{lay_{i,j}}$):

$$Q_{AC} = \sum_{i}^{3} \sum_{j}^{nl_i} \int_{0}^{L_{lay_{i,j}}} \left[\frac{\mu_0 f}{\pi} I_c(x)\, \xi_{i,j}(x) \right] dx \tag{3}$$

$$L_{lay_{i,j}} = Tapes_{i,j} \frac{d_{stat}}{\left| cos(\alpha_{i,j}) \right|} \tag{4}$$

$$\begin{aligned} \xi_{i,j}(x) = &\big(1 - F_{i,j}(x)\big) \ln\big(1 - F_{i,j}(x)\big) + \\ &+\big(1 + F_{i,j}(x)\big) \ln\big(1 + F_{i,j}(x)\big)\, F_{i,j}^2(x) \end{aligned} \tag{5}$$

$$F_{i,j}(x) = \frac{I_{M_{i,j}}}{I_c(x)} = \frac{\sqrt{2}\, \left| \underline{I_{i,j}} \right|}{Tapes_{i,j}\, I_c(x)} \tag{6}$$

$$Tapes_{i,j} = round\left(\frac{2\pi\, R_{i,j}\, \left| cos(\alpha_{i,j}) \right|}{w_{HTS}} \right) \tag{7}$$

where f is the operating frequency (50 – 60 Hz), μ_0 is the vacuum permeability and $F_{i,j}$ is the ratio between I_c and the amplitude of the current flowing in each tape of the j^{th} layer of the i^{th} phase, $I_{M_{i,j}}$. The current $I_{M_{i,j}}$ is computed assuming that the tapes belonging to the same layer are in parallel electrical connection and that the layer current ($\underline{I_{i,j}}$) is equally shared between

them. Both I_c and $F_{i,j}$ are here expressed as functions of the coordinate x, and are computed from the user-defined $I_c(T_{HTS})$ function, depending on the tape selected. Finally, $L_{lay_{i,j}}$ and $Tapes_{i,j}$ are the total tape length included in a cable segment and the number of tapes needed to wind the j^{th} layer of the i^{th} phase. w_{HTS} is the tape width and $R_{i,j}$ is the inner radius of the selected layer. In (7), the function $round$ approximates the result to the nearest integer.

Eq. (5) is written for tapes having a rectangular cross-section, but the equation referring to conductors with an elliptical cross-section (described in [27]), is also implemented in the model. Depending on the kind of tape selected for the study, the proper equation is adopted.

B.Losses in the dielectric

Compared to the formula used to calculate the losses in the electrical insulation of single-core cables [34], for each insulating layer of a coaxial cable, the line voltage (V_{rms}) must be taken into account rather than the phase voltage:

$$Q_{ins} = \sum_{w}^{3} (2\,\pi\, f\, d_{stat}\, tan\delta_{ins}\, Capac_m\, V_{rms}^2) \tag{8}$$

$$Capac_m = 2\,\pi\,\varepsilon_{ins}\,\varepsilon_0 \ln\left(\frac{R_{ext_{ins\,m}}}{R_{int_{ins\,m}}}\right) \tag{9}$$

where $tan\delta_{ins}$ and ε_{ins} are the loss tangent and the permittivity of the selected dielectric. Generally, for superconducting cables, the insulating material selected is laminated polypropylene paper (PPLP). ε_0 is the vacuum permittivity and $Capac_w$ is the capacitance of the m^{th} insulating layer of the cable. $R_{int_{ins\,m}}$ and $R_{ext_{ins\,m}}$ are the inner and outer radii of the m^{th} insulating layer. $R_{int_{ins\,m}}$ is computed knowing the inner radius and the thickness of the underlying superconducting layer. $R_{ext_{ins\,m}}$ depends on the thickness of each insulating layer, whose calculation is reported in Chapter IV.

C.Heat from the cryostat

In the literature, the calculation of the cryostat thermal load in HTS cables is performed both using analytical formulae [22, 35] and empirical values per unit of length [26, 34 – 38]. The choice between flexible and rigid cryostats is relevant. The former generally involve greater thermal inputs due to the presence of corrugated stainless-steel tubes, but improve the mechanical flexibility to the cable. In [34] it is reported that the thermal load can be 70% greater for flexible cryostats compared to rigid ones, with the same diameter. In this study, Q_{cryo} is computed as follows [35] for a flexible cryostat:

$$Q_{cryo} = d_{stat}\frac{2\pi\,\lambda\left[T_a - \left(T_{max_{an}} + T_0\right)/2\right]}{\ln(R_{cryo_{ext}}/R_{cryo_{int}})} \tag{10}$$

where λ is the "effective" cryostat thermal conductivity (equivalent to that for MLI) and T_a is the average ambient temperature during the year at the cable installation site. $R_{cryo_{ext}}$ and $R_{cryo_{int}}$ are the outer and inner radii of the cryostat, respectively. $R_{cryo_{int}}$ is known from the inner radius of the annular gap and its thickness t_{an}, while $R_{cryo_{ext}}$ depends on $R_{cryo_{int}}$ and the thickness of the cryostat walls (t_{cryo}), imposed by the user.

Adopting a value of λ of 0.3 mW/m·K, in accordance with reported ranges [39 – 42], a cryostat thickness of 2 cm and a T_r value of 293 K, the resulting values of Q_{cryo}, once divided by d_{staz}, are within the ranges provided by other publications [26, 34 – 37], generally included in the range from 1 to 2 W/m.

D.Eddy current terms

The eddy current losses (Q_{ed}) that occur in normal conducting materials are computed from the corresponding value q_{ed}, which is expressed per unit length and is a function of the amplitude of the design current of the cable [3]. This loss contribution is generally significantly lower than the others.

IV.FUNCTION FOR THE DIELECTRIC THICKNESS

The insulation design method is based on checking that the three dielectric layers present in a concentric cable can withstand two distinct electrical stress conditions: the AC nominal voltage and the lightning impulse voltage [43 – 46]. For the m^{th} insulating layer, the following values are computed, and the major one is adopted in the cable design:

$$t_{ins_{AC_m}} = R_{int_{ins\,m}}\left[exp\left(\frac{k_{1_{AC}}\,k_{2_{AC}}\,k_{3_{AC}}\,V_{AC}}{R_{int_{ins\,m}}\,E_{AC}}\right) - 1\right] \tag{11}$$

$$t_{ins_{im_m}} = R_{int_{ins\,m}}\left[exp\left(\frac{k_{1_{im}}\,k_{2_{im}}\,k_{3_{im}}\,V_{im}}{R_{int_{ins\,m}}\,E_{im}}\right) - 1\right] \tag{12}$$

where $k_{1_{AC}}$ and $k_{1_{im}}$ are the corrective ageing coefficients, to compensate for the degradation of the dielectric properties under electric stress that may occur during the years of operation. $k_{2_{AC}}$ and $k_{2_{im}}$ are the corrective temperature coefficients, taking into account the possible insulation failure due to the heat aging. However, since the operating temperature in the insulating layers of a superconducting cable are generally way lower than those occurring in a conventional cable, the temperature coefficients are generally close to unit. $k_{3_{AC}}$ and $k_{3_{im}}$ are the correction safety coefficients, which can be used as design safety margins [43 – 46]. V_{im} is the lightning impulse target withstand voltage and V_{AC} is the AC rated voltage, usually calculated as 2.5 $(\sqrt{2}V_{rms})/\sqrt{3}$ according to IEC 62067 [46, 47]. E_{AC} and E_{im} are the breakdown voltages for both conditions. These parameters refer to the specific dielectric material selected, and can be found in the literature.

V.DEFINITION OF THE PROBLEM CONSTRAINTS

The proposed model solves a minimization problem by imposing multiple electrical and physical constraints to the cable configuration.

First, the tool computes the current distribution between the individual phases, layers and tapes. To simplify the discussion, the HTS tapes belonging to the same layer are assumed to be in parallel, and the layer current ($\underline{I_{i,j}}$) is assumed to be equally shared between them. It is supposed to insert the cable into a grid to connect a direct symmetrical three-phase generator system to a three-phase wye connected load. The following system of equations is solved to determine the layer currents $\underline{I_{i,j}}$:

$$\begin{cases} \dfrac{V_{rms}}{\sqrt{3}} = \sum_{i=1}^{3}\sum_{j=1}^{nl_i} j\omega\, M_{1,k-i,j}\,\underline{I_{i,j}} + \sum_{j=1}^{nl_1} Z_L\,\underline{I_{1,j}} + \underline{V_s} \\ \qquad\qquad for\ k = 1, \dots, nl_1 \\ \dfrac{V_{rms}}{\sqrt{3}}\, e^{-j\frac{2}{3}\pi} = \sum_{i=1}^{3}\sum_{j=1}^{nl_i} j\omega\, M_{2,k-i,j}\,\underline{I_{i,j}} + \sum_{j=1}^{nl_2} Z_L\,\underline{I_{2,j}} + \underline{V_s} \\ \qquad\qquad for\ k = 1, \dots, nl_2 \\ \dfrac{V_{rms}}{\sqrt{3}}\, e^{j\frac{2}{3}\pi} = \sum_{i=1}^{3}\sum_{j=1}^{nl_i} j\omega\, M_{3,k-i,j}\,\underline{I_{i,j}} + \sum_{j=1}^{nl_3} Z_L\,\underline{I_{3,j}} + \underline{V_s} \\ \qquad\qquad for\ k = 1, \dots, nl_3 \\ \sum_{i}^{3}\sum_{j}^{nl_i} \underline{I_{i,j}} = 0 \end{cases} \quad (13)$$

where $M_{1,k-i,j}$, $M_{2,k-i,j}$ and $M_{3,k-i,j}$ are the mutual inductances of the layers belonging to the 1st, 2nd and 3rd phases, respectively. Z_L is the impedance of the three-phase load and $\underline{V_s}$ is the voltage of the common wye node.

The impact of the equivalent longitudinal resistance of the superconducting layers on the current distribution is assumed negligible, and therefore it does not appear in (13).

The inductances are computed as in [48 – 50]:

$$M_{1,k,j,j} = L_{line}\frac{\mu_0}{4\pi}\left[2\,ln\left(\frac{R_n}{R_{i,j}}\right) + \frac{R_{1,k}}{R_{i,j}}tan(\alpha_{1,k})\,tan(\alpha_{i,j})\right] \quad (14)$$

where R_n is the radius of the copper neutral conductor, known once the radius of the underlying insulation layer is determined through the optimization procedure.

For what concerns the load (included in (13) to impose a certain operation current of the cable), Z_L is calculated as:

$$Z_L = \frac{{V_{rms}}^2\cos\varphi}{P} \quad (15)$$

where $\cos\varphi$ is the load factor and P is the active power used to size the cable.

Then, the following constraints are applied to currents and other cable parameters.

A. Constraints on the phase and layers currents

The phase currents resulting from the optimized cable configuration have to form a balanced three-phase system. In the tool, this is verified by imposing that the relative difference of each phase current with respect to the design value I_{rms} (perfectly balanced current) is lower than a limit value set by the user ($\%_{max_{ph}}$):

$$\left|\left|\sum_{j=1}^{nl_i}\underline{I_{i,j}}\right| - \left(\frac{I_{rms}}{nl_i}\right)\right| \Big/ \left(\frac{I_{rms}}{nl_i}\right) \le \%_{max_{ph}}\ for\ i = 1,2,3 \quad (16)$$

$$I_{rms} = \frac{P}{\sqrt{3}\,V_{rms}\cos\varphi} \quad (17)$$

In the same way, each phase current should be equally distributed among its constituting superconducting layers. That would avoid having layers working at currents closer to the critical value (with higher AC losses) and other underloaded layers. This is accomplished by imposing the following constraints to the layer currents:

$$\frac{\left|\left|\underline{I_{i,j}}\right| - \left|\underline{I_{i,j+1}}\right|\right|}{max\left(\left|\underline{I_{i,j}}\right|, \left|\underline{I_{i,j+1}}\right|\right)} \le \%_{max_{lay}} \begin{cases} for\ i = 1,2,3 \\ for\ j = 1, \dots, nl_i - 1 \end{cases} \quad (18)$$

where $\%_{max_{lay}}$ is the limit imposed by the user for the relative difference between the module of a given layer current and the module of the other layer currents of the same phase.

B. Constraint on the maximum currents in the HTS tapes

Generally, any superconducting device should not exceed a given safety criterion on the maximum operating current flowing in the superconducting material compared to its critical current. In the case of a coaxial cable, this represents a constraint on the amplitude of the layer current $\left|\underline{I_{i,j}}\right|$, since all its constituting tapes have the same I_c. Also, since the superconductor temperature varies along the segment included between two adjacent cooling stations, so does the tape critical current. As a conservative choice, the lowest I_c value in a cable segment is taken as a reference. This value, referred to as $I_{c_{min}}$, corresponds to the lower between those computed at $T_{HTS_{left}}$ and $T_{HTS_{right}}$: $I_{c_{min}} = I_c\left(max\left[T_{HTS_{left}}, T_{HTS_{right}}\right]\right)$ Thus, the following constraint is imposed to all layer currents:

$$\frac{\sqrt{2}\,\left|\underline{I_{j,h}}\right|}{Tapes_{i,j}} \le I_{c_{min}} sf_{HTS} \quad \begin{cases} for\ i = 1,2,3 \\ for\ j = 1, \dots, nl_i - 1 \end{cases} \quad (19)$$

where sf_{HTS} is the safety criterion (generally ranging from 0.5 to 0.9) set by the user.

C. Constraint on the line voltage drop

To ensure that the loads connected to the cable can operate at a voltage level close to their design value, the voltage drop across the whole cable length has to be lower than a certain maximum percentage of the design voltage V_{rms}, imposed by the user and generally dependent on grid regulations. Being the superconducting layers in parallel within the same phase, the

check has to be performed for each of them. Neglecting the equivalent longitudinal resistance of the superconductor, the following mathematical constraint can be imposed to all layers:

$$\frac{\omega \left| [M] \cdot \left[\underline{I_{i,j}} \right] \right|}{V_{rms}} \leq \%_{max_{Vdrop}} \quad \begin{cases} for\ i = 1,2,3 \\ for\ j = 1, \dots, nl_i - 1 \end{cases} \tag{20}$$

where $\%_{max_{Vdrop}}$ is the voltage drop limit selected by the user, $[M]$ and $\left[\underline{I_{i,j}}\right]$ are the mutual inductances matrix, defined in (14), and the layer currents vector, which can be found solving (13).

D. Constraints on coolant temperature and pressure

The coolant flowing in the pipes between two adjacent cooling stations is subjected to pressure drops and temperature rises due to both friction and absorbed heat. These variations must be carefully monitored to ensure that the cryogen maintains its thermal properties along the whole cable length. In particular, for liquid nitrogen, it must remain in the subcooled liquid phase to avoid vapor bubbles formation, which would limit its heat exchange. Hereafter, liquid nitrogen will be referred to as the cryogen for this study, but the methodology described is also valid for other coolants, taking into account their proper fluid-dynamic constraints. In particular, at the operating temperatures of the HTS cable, nitrogen can be considered as an incompressible fluid and its pressure and temperature profiles along the cable length can be computed via relatively simple analytic formulae, with a reasonable approximation. Moreover, due to the limited temperature variations to which nitrogen can be subjected in the cable, its density (ρ_{LN2}), specific heat capacity (cp_{LN2}) and dynamic viscosity (μ_{LN2}) are approximated as constants, using their average values within the operating temperature and pressure ranges chosen.

Then, the following constraints are imposed regarding the pressure drop (ΔP) and temperature rise (ΔT) in both the former and the annular gap. To improve readability, the formulae for a generic pipe having a hydraulic radius R_h are given. For the former, this corresponds to R_f, while for the annular gap it corresponds to t_{an}. The subscript h can either indicate the former or the annular gap.

$$\Delta P_h = \left(d_{stat} \frac{\rho_{LN2}\, {v_{LN2_h}}^2\, f_{LN2_h}}{4\, R_h} \right) + (g \rho_{LN2} \Delta h) \leq \Delta P_{LN2_{max}} \tag{21}$$

$$\Delta T_h = d_{stat} \left(\frac{{v_{LN2_h}}^2\, f_{LN2_h}}{4\, R_h\, cp_{LN2}} + \frac{Q_h}{2\, \dot{m}_{LN2}\, cp_{LN2}} \right) \leq \Delta T_{LN2_{max}} \tag{22}$$

$$v_{LN2_h} = \frac{\dot{m_{LN2}}}{\rho_{LN2}\, \pi\, {R_h}^2} \tag{23}$$

$$f_{LN2_h} = \left\{ -1.8 \ln \left[\left(\frac{\varepsilon_h}{7.4\, R_h} \right)^{1.11} + \left(\frac{6.9}{Re_h} \right) \right] \right\}^{-2} \tag{24}$$

$$Re_h = \frac{2\, R_h\, v_{LN2_h}\, \rho_{LN2_h}}{\mu_{LN2}} \tag{25}$$

where v_{LN2_h}, f_{LN2_h} and Re_h are the velocity, the friction factor and the Reynolds number of the fluid flowing in the pipe h, respectively, while ε_h is the roughness of the pipe itself. $\Delta P_{LN2_{max}}$ and $\Delta T_{LN2_{max}}$ are the maximum pressure drop and temperature rise imposed by the user, dependent on temperature (T_0) and pressure (P_0) of the nitrogen exiting from each cooling station. g is the gravity acceleration and Δh is the height difference between the two ends of a cable segment (assumed equal for all cable segments) [34].

The expression reported in (24) is computed approximating the implicit Colebrook-White equation for corrugated cylindrical tubes [51] and using the Haaland explicit equation [52].

Furthermore, the circular cross-sections of the inner and outer walls of the annular gap are considered to be concentric in this study. However, it is possible to include this design option in the model by entering a correction factor for the cable eccentricity in the friction factor $f_{LN2_{an}}$, as described in [53].

It is worth noting that applying (22) to the former and the annular gap results in two implicit equations, given that both the losses Q_f and Q_{an} depend on the maximum temperatures of the nitrogen in the two flows, as described in (2).

E. Other constraints

The model computes the parameter $Tapes_{i,j}$ as described in (7); then, a check is performed on the resulting gap between adjacent tapes belonging to the same layer ($g_{i,j}$). The function to calculate the gap depends on $Tapes_{i,j}$, $R_{i,j}$ and $\alpha_{i,j}$, as shown in [54]. For each superconducting layer, the gap should not exceed 3% of w_{HTS} so as to minimize the transverse component of the magnetic field acting on each tape (produced by the tape itself and by the adjacent ones) and the resulting magnetization losses [55]. If this condition is not respected, $Tapes_{i,j}$ is increased by one unit and the check is performed again.

Finally, among the parameters selected for the optimization (listed in Chapter II.A), nl_i and n_{stat} must correspond to positive integers, while the other parameters can be rational numbers. In the MATLAB code, the *ga* algorithm allows one to easily select which parameters must respect this constraint.

VI. Description of the Cost Function

The proposed tool returns the cable design that minimizes the costs; thus it is essential to determine a valid objective function for the superconducting cable system. In the literature, there is a limited number of examples for estimating these costs [22, 53, 56 – 63], each considering specific indexes. The objective function presented here contains the elements for the cost calculation depending on the cable design and operating conditions. The parameters are adapted from those found in other publications, but the user can modify them to carry out parametric analyses. In the following, when a cost index is expressed with the uppercase letter (C) it indicates the total cost, while the use of a lower case letter (c) represents the unitary cost.

The total cost for the cable system (C_{tot}) is computed as follows:

$$C_{tot} = C_{HTS} + C_{ins} + C_{LN2} + C_{cool} + C_{cryo} + C_{vac} + C_{ter} + C_{cab} + C_{lay} + C_{man} + C_{dis} \quad (26)$$

where C_{HTS}, C_{ins} and C_{LN2} are the costs for the superconducting material, for the electrical insulation and for the liquid nitrogen, respectively. C_{cool}, C_{cryo}, C_{vac}, and C_{ter} are the costs for the cooling stations (including coolers and circulation pumps), the cryostat, the vacuum pumps system and the cable terminations, respectively. C_{cab}, C_{man}, C_{dis} and C_{lay} are the cabling, laying maintenance and dismantling costs, respectively. These cost indexes are described in detail in the next Sections.

A.Superconducting material cost

C_{HTS} can be computed as:

$$C_{HTS} = c_{HTS} \sum_{i}^{3} \sum_{j}^{nl_i} Tapes_{i,j} \frac{L_{line}}{|cos(\alpha_{i,j})|} \quad (27)$$

where c_{HTS} is the tape cost per unit of length.

B.Electrical insulating material cost

C_{ins} is calculated as follows:

$$C_{ins} = c_{ins}\, \rho_{ins}\, L_{line}\, \pi \sum_{w}^{3} \left({R_{ext_{ins\,w}}}^2 - {R_{int_{ins\,w}}}^2 \right) \quad (28)$$

where c_{ins} is the insulation cost per unit of weight, ρ_{ins} is the insulation mass density, and $R_{ext_{ins\,m}}$ is the outer radius of the m^{th} insulating layer (computed knowing $R_{int_{ins\,m}}$ and solving (11)-(12)).

C.Cryogenic fluid cost

The following formula is used to compute C_{LN} :

$$C_{LN2} = c_{LN2}\, L_{line}\, \pi \left[{R_{ext_{an}}}^2 - {R_{int_{an}}}^2 + \left(R_f - t_f\right)^2 \right] \quad (29)$$

where c_{LN2} is the cost of liquid nitrogen per unit of volume and t_f is the former thickness (which includes the former roughness ε_f). $R_{ex\ an}$ and $R_{int_{an}}$ are the outer and inner radii of the annular gap. $R_{in\ an}$ is known from the radius (R_n) and the thickness (t_n) of the underlying copper neutral layer, while $R_{ext_{an}}$ depends on $R_{int_{an}}$ and the thickness t_{an}.

D.Cooling stations cost

The cost of all the cooling stations is calculated as:

$$C_{cool} = \sum_{k}^{n_{staz}+2} C_{op_k} + C_{cap_k} \quad (30)$$

$$C_{op_k} = \sum_{z}^{yr} c_{kWh} h_y \left[\left(\frac{Q_{c_k}}{\eta_{cry}} \frac{(T_a - T_0)}{T_0} \right) + \frac{Q_{p_k}}{\eta_p} \right] \frac{1}{(1+\psi)^z} \quad (31)$$

$$C_{cap_k} = C_{cool_{fixed}} + \left[\left(c_{cryocooler}\, Q_{c_k} \right) \beta_Q \right] \beta_r \quad (32)$$

$$Q_{c_k} = \begin{cases} Q_f + Q_{an} & if\ k = intermediate\ stat. \\ Q_{an} + Q_{cl} & if\ k = left\ termination\ stat. \\ Q_f + Q_{cl} & if\ k = right\ termation\ stat. \end{cases} \quad (33)$$

$$Q_{p_k} = \begin{cases} m_{LN2} \dfrac{\Delta P_f + \Delta P_{an}}{\rho_{LN2}} & if\ k = intermediate\ stat. \\ \dfrac{\dot{m_{LN2}}\, \Delta P_{an}}{\rho_{LN2}} & if\ k = left\ termination\ stat. \\ \dfrac{\dot{m_{LN}}\, \Delta P_f}{\rho_{LN2}} & if\ k = right\ termation\ stat. \end{cases} \quad (34)$$

where C_{cap_k} and C_{op_k} are the capital and operating costs of the k^{th} cooling station.

As for the operating costs, yr are the years of service expected for the system and c_{kW} is the actual energy cost for non-household consumers in the region where the cable is planned to be located. h_y are the hours of service per year; assuming the cable to operate continuously, h_y is the number of hours in a year. Q_k is the heat which must be removed from the cryogenic fluid by each cooling station (sum of the contributions of each inlet flow to the station, as explained in Chapter III), whose efficiency is equal to η_{cry}. Q_{p_k} is the hydraulic power delivered by the circulation pumps to the liquid nitrogen flows to restore their pressure after the drops computed with (21) (ΔP_f and ΔP_{an} for the nitrogen flowing in the former and in the annular gap, respectively). Compared to intermediate stations, the termination stations must restore the pressure in a single inlet flow. η_p is the efficiency of the circulation pumps and ρ_{LN2} is the density of liquid nitrogen [63]. The temperature ratio in (31) corresponds to the inverse Carnot efficiency [34]. ψ is the annual effective discount rate for the operating costs, which depends on the country where the cable is expected to be located. It is worth noting that inflation could also be taken into account when computing the operating costs in (31). To give an indication, in Europe the mean annual inflation for the cost of electric energy was equal to 2.3% from 2009 to 2020, with a non-linear trend [64]. However, its long-term estimate is not trivial and often depends on unpredictable factors. In this work, the inflation was excluded from the calculations.

For what concerns the capital costs, the term $c_{cryocooler}$ is the cost of the cryocoolers system per unit of power to be extracted (Q_k). β_Q is a mark-up introduced to consider that the cooling system should handle possible heat peaks and to account for the practical impossibility to find in the market devices of the exact size required (in these cases, the superior size is selected). β_r is a mark-up adopted to consider the cost of the cooling station devices for which no parametric function has been found (circulation pumps, LN_2 tank and accessory components). It is assumed that these costs correspond to a certain percentage of the cryocooler cost. $C_{cool_{fixed}}$ takes into account the fixed costs required for each cooling station besides the device cost (installation, maintenance, disposal, etc.).

It is worth noting that, in this study, the cooling system is not designed with redundancy. However, an extra mark-up could be added to (32) to account for this possible design choice.

E. Other cost terms

Finally, the terms C_{cryo}, C_{vac}, C_{ter}, C_{cab}, C_{man}, C_{dis} and C_{lay} in (26) are computed by multiplying the corresponding values reported in the literature per unit of cable length (indicated as c_{cryo}, c_{vac}, c_{ter}, c_{cab}, c_{man}, c_{dis} and c_{lay}, respectively) by L_{line}.
In particular, C_{man} can be accounted as an operating cost, and its value must be discounted:

$$C_{man} = \sum_{z}^{yr} \frac{L_{line}\, c_{man}}{yr\,(1+\psi)^{z}} \tag{35}$$

C_{dis} must also be discounted, as it refers to the end of the cable service period. Thus, this cost is multiplied by $(1+\psi)^{-y}$.

In this work, the superconducting solution is supposed to replace an existing conventional line and the required tunnels can be retrofitted. Therefore, excavation costs, cable trench and wiring ducts are avoided. However, if the retrofitting is not possible, and a new line is designed, their approximate values can be set as reported in the literature (see for example [63]) and added in (26).

VII. Reference values for the analysis

In order to present in Chapter VIII the results of some parametric analyses, the investigation limits and the user-defined (non-optimizable) parameters selected in the study are reported in this chapter.

A. Upper and lower boundaries for the system variables

Upper and lower limits should be set for each variable of the problem, and are listed in Chapter II.A. This directs the optimization process towards a local minimum that falls within the range of interest. However, a poor selection of the limits can prevent the algorithm from finding a solution that satisfies the constraints. With the aim of realizing a parametric analysis over a wide spectrum of operating conditions, it is useful to keep these ranges as broad as possible.
In this respect, the boundaries shown in Table I are selected for this study.

TABLE I
Upper and lower boundaries for the system variables

Parameter	Unit	Lower boundary	Upper boundary
R_f	[cm]	1.0	2.5
t_{an}	[cm]	1.0	3.0
nl_i		1	5
$\alpha_{i,j}$	[°]	$-\pi/6$	$\pi/6$
$\dot{m}_{LN2}$	[Kg/s]	0.2	2.0
n_{stat}		0	$round(L_{line}/1e3) - 1$

B. Genetic algorithm options selected in MATLAB

MATLAB allows to set specific options for the *ga* algorithm which can impact its speed and/or lead to a better solution. Table II reports the values selected for the main algorithm options, after performing a convergence study to reduce the computation times. MATLAB default values are used for the remaining parameters not mentioned in this chapter.

TABLE II
Algorithm options selected in MATLAB

MATLAB *ga* option	Value
PopulationSize	100
FunctionTolerance	1e-9
ConstraintTolerance	1e-4

More specifically, Table III shows the impact of the parameter *PopulationSize* (the number of individuals of each population) on the computation time. Since the whole genetic algorithm runs multiple times consecutively, Table III displays the data referring to the less time-consuming iterations whose corresponding fitness value is within 0.1 ‰ from the lowest fitness value found in all iterations (*i.e.* the fastest iteration leading to the best solution).

TABLE III
Impact of the population size on the computational time

PopulationSize	N°generations	Computational time per generation [s]	Total computational time [s]
50	277	2.1	578.0
100	194	4.1	801.0
150	157	6.3	993.0
200	147	8.2	1212.5
250	136	9.9	1344.4
300	123	12.0	1476.4

As expected, as the number of individuals increases, the amount of generations required to achieve the same best fitness value is reduced. However, the computation time required to pass from one generation to the next one increases more rapidly, and as a result the total computation time for the whole genetic algorithm increases with *Populationsize*. The size of population equal to 50 is excluded, as it is considered too small with respect to the number of variables involved (which can vary from 10 to 22, depending on the value of nl_i). A value of *Populationsize* equal to 100 is selected as a good compromise between speed and quality of the algorithm.

Finally, as for the initial population for the genetic algorithm, the genes of each individual are set equal to the arithmetic mean between the upper and lower boundaries of the corresponding variables, reported in Table I.

C. Constraint parameters

Table IV reports the limits for the problem constraints selected in this work. These thresholds depend on operational choices and physical or regulatory limits to be respected.

TABLE IV
CONSTRAINTS PARAMETERS SELECTED FOR THE ANALYSIS

Parameter	Unit	Value	Reference
$\%_{max_{ph}}$	%	0.8	
$\%_{max_{lay}}$	%	0.1	
sf_{HTS}		0.7	
$\%_{max_{Vdrop}}$	%	4.0	[65]
$\Delta P_{LN2_{max}}$	bar	12	[24]
$\Delta T_{LN2_{max}}$	K	10	
T_0	K	68	
P_0	bar	15	

D. Dielectric parameters

PPLP is selected as the dielectric between conductive phases. Its properties at liquid nitrogen temperature, as well as the parameters reported in Chapter IV, are presented in Table V.

TABLE V
DIELECTRIC PARAMETERS SELECTED FOR THE ANALYSIS

Parameter	Unit	Value	Reference
$tan\delta_{ins}$		6e-4	[66]
ε_{ins}		2.21	[67]
ρ_{ins}	ton/m^3	0.9	[68]
V_{im}	kV	150	[44]
E_{im}	MV/m	76	
E_{AC}	MV/m	52	
$k_{1_{AC}}$		1.59	
$k_{1_{imp}}$		1.32	
$k_{2_{AC}}$, $k_{2_{imp}}$		1.0	
$k_{3_{AC}}$		1.45	
$k_{3_{imp}}$		1.0	

E. Cost parameters

Table VI presents the cost parameters selected for this study.

TABLE VI
COST PARAMETERS SELECTED FOR THE ANALYSIS

Parameter	Unit	Value	Reference
c_{HTS}	€/m	35.0	
c_{ins}	M€/ton	0.01	[44]
c_{LN2}	€/liter	1.0	
c_{cryo}	€/W	100.0	[69]
c_{vac}	€/m	52.0	[70]
c_{cab}	M€/m	3.0	[71]
c_{ter}	M€/m	0.06	[72]
c_{man}	M€/m	0.01	
c_{dis}	M€/m	0.02	
c_{lay}	M€/m	0.02	
$C_{cool_{fixed}}$	M€	0.2	
β_Q		1.1	
β_r		1.1	
ψ	%	0.1	
yr		40	

F. Other user-defined parameters selected for the analysis

For the analysis, the geometric, electrical and cost parameters of the HTS *SuNAM SCN04* tape are considered [73]. For this tape, w_{HTS} and t_{HTS} are equal to 4.1 mm and 150 µm respectively. The $I_c(T_{HTS})$ function is taken from [74]. It is worth noting that, in the limited temperature range at which the superconductor operates in this study (assuming self-field conditions), the tape I_c can be approximated as a linear function of the temperature.

Finally, the remaining user-defined parameters selected for the analysis are reported in Table VII.

TABLE VII
OTHER PARAMETERS SELECTED FOR THE ANALYSIS

Parameter	Unit	Value	Reference
ε_h	mm	1.4	[34]
η_p		0.7	
Δh	m	1.0	
t_f	mm	2.0	
t_{lev}	mm	1.9	[26]
t_c	mm	0.8	
t_n	mm	3.0	[24]
t_{cryo}	cm	2.0	
t_k	µm	50.0	
η_{cry}		0.1	[46]
ρ_{LN2}	kg/m^3	839.0	
cp_{LN2}	J/kg·K	2662.0	
μ_{LN2}	µPa·s	25.08	
q_{cl}	W/kA per current lead	45.0	[3]
q_{ed}	W/kA·m	0.05	
T_r	K	293.0	

VIII. RESULTS OF THE PARAMETRIC ANALYSIS

This Chapter presents the results of several explicative parametric analyses performed with the proposed tool. Cost trends and optimized cable configurations are shown, underlining how different technical-economic aspects are related to each other.

A. Impact of the cable active power

In this study, a 5 km long cable is connected to a load with $cos\varphi$ = 0.9, at a voltage level equal to 15 kV. The simulations are performed multiple times varying the active power in the range from 50 MW to 200 MW, with 25 MW steps, so as to find the optimized cable configurations.

In the following bar charts, the arrangement of the bars into each column matches the order in which the terms are presented in the legend (top to bottom). Furthermore, the numerical references of the bars with respect to the legend are highlighted in the last column of the graphs.

Fig. 5(a) shows the total capital cost of the system per kilometer of cable. As expected, as the required power increases, the system cost rises. However, this increase is not constant

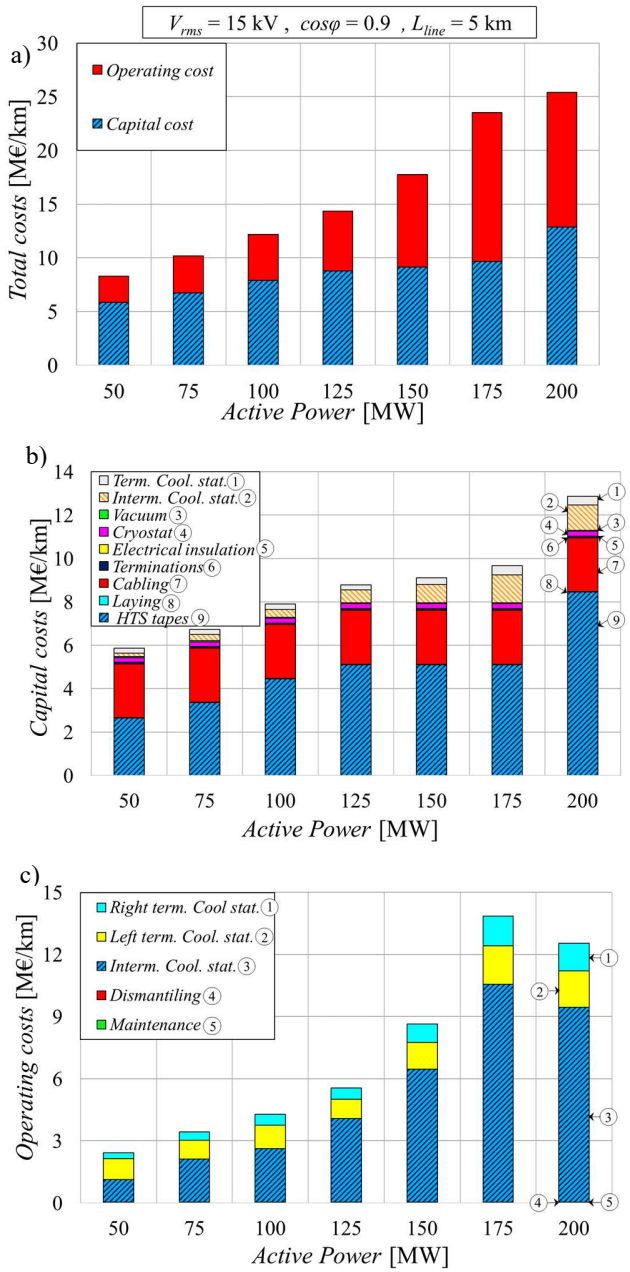

Fig. 5. (a) Total, (b) capital and (c) operating costs per kilometer of cable varying the active power. The case considered has V_{rms} = 15 kV, $cos\varphi$ = 0.9 and L_{line} = 5 km.

with the active power: it is approximately linear for power values up to 125 MW, then it rises more steeply up to 175 MW. Finally, the rise in cost between 175 MW and 200 MW is lower compared to the previous ones. Furthermore, the ratio between capital and operating costs (over a 40-year period) is not constant increasing *P*. Operating costs exhibit a stronger dependence on power than capital costs, reaching, and in some cases exceeding, 50% of the total costs.

Fig. 5(b) shows the different contributions to the capital costs, for the various cases analysed. In particular, the following cost indexes are included in the capital costs: HTS tapes,

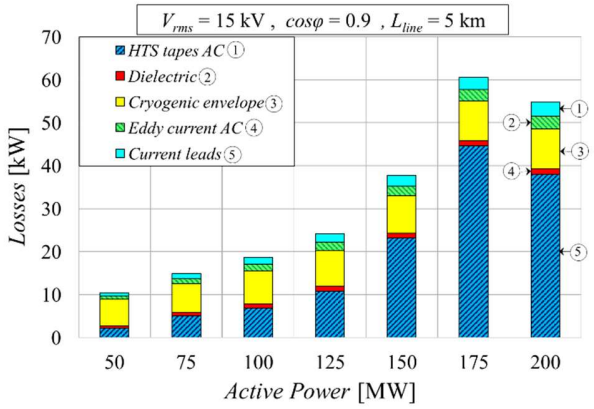

Fig. 6. Losses and heat inputs along the whole cable length varying the active power. The case considered has V_{rms} = 15 kV, $cos\varphi$ = 0.9 and L_{line} = 5 km.

cabling and laying, vacuum system and cryostat, terminations and cooling stations, distinguishing between intermediate and termination ones. It is worth noting that the dielectric, laying and termination costs are almost negligible, while the cost to purchase the HTS tapes, for cabling and for the cooling stations are predominant. While cabling costs are set constant per unit of cable length, the costs of the HTS tapes increase between 50 and 75 MW, then remain almost constant up to 175 MW and finally rapidly grow to 200 MW, reaching 2/3 of the capital costs of the cable.

Fig. 5(c) presents the different contributions to the operating costs. In particular, the following items are included in the operating costs: maintenance and dismantling costs of the system, and operating costs of the intermediate and termination cooling stations, distinguishing between the termination station located at the left and right side of the cable. The increase in the operating costs is approximately quadratic up to 175 MW; then, the costs slightly drop from 175 MW to 200 MW.

It is worth noting that the impact over the total operating costs of the intermediate cooling stations increases compared to that of the termination stations as the active power rises; in fact, the number of intermediate stations needed increases. The same applies to operating costs. Furthermore, the costs of the left termination station are always higher than those of the right one. In fact, by combining (2) and (33), it results that the termination station located at the left side of the cable must manage a higher amount of thermal power than the one on the right side.

To better understand these trends, it is useful to refer to other quantities.

Fig. 6 shows the sum of losses and the heat inputs along the whole cable length, for the same cases of Fig.5. Their trend with increasing the active power closely follows that of the operating costs shown in Fig. 5(c); indeed, the operating costs are approximately linearly dependent on losses, as shown in (31).

While the dielectric losses are almost constant since the rated voltage does not vary, the current lead losses and the eddy current AC losses are proportional to the operation current, which increases linearly with the active power.

The heat entering from the cryostat rises linearly with the active power. In fact, on the one hand, as the losses grow, the average

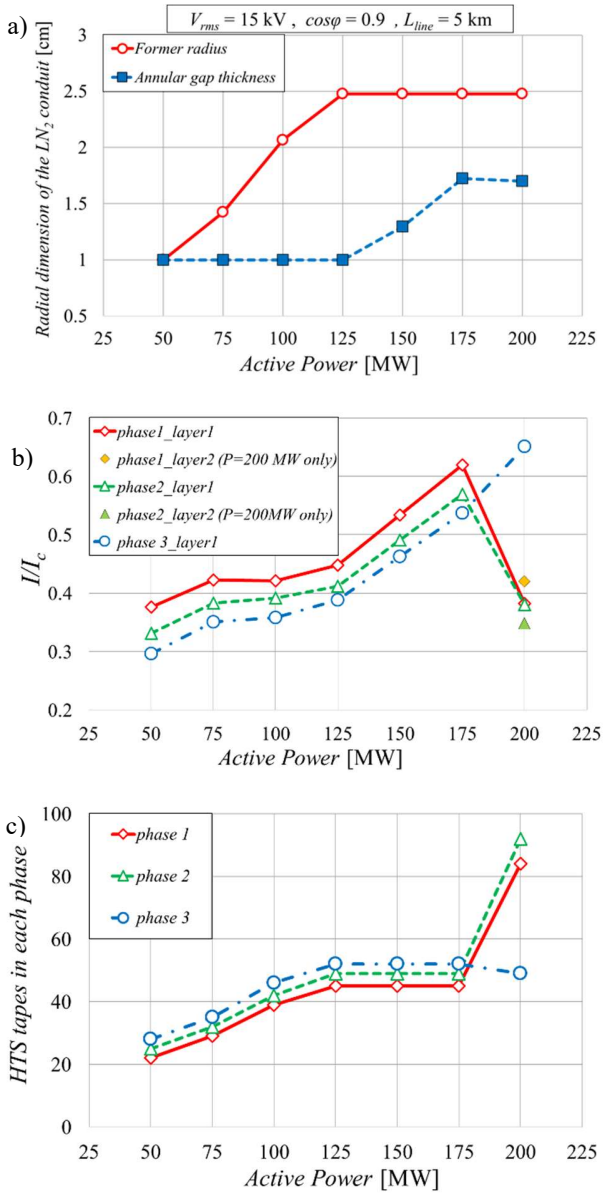

Fig. 7. (a) Parameters R_f and t_a, (b) I/I_c ratio in each layer of the three phases and (c) sum of the HTS tapes used to wind each phase of the cable, varying the active power. The case considered has V_{rms} = 15 kV, $cos\varphi$ = 0.9 and L_{line} = 5 km.

temperature of the nitrogen in the annular gap rises, which causes an increase in the numerator in (10). On the other hand, while the thickness of the cryostat remains constant, the ratio between the external and internal radius of the cryostat decreases and so does the denominator in (10). It appears evident that the reduction in total losses and operating costs between 175 MW and 200 MW is due to a reduction in HTS AC losses.

In Fig. 7(a), the parameters R_f and t_a are displayed. At 50 MW, both the optimized geometrical parameters are equal to the lower boundary set by the user (1 cm). In this way, the radii of the superconducting layers are minimized so as the number of tapes and the consequent capital cost. Furthermore, a low t_a value reduces the radial dimensions of the cryostat and consequently the surface which can be irradiated from outside. Then, the radius of the former increases with increasing power, until it reaches the upper boundary set by the user (2.5 cm) for a power of 125 MW. For larger power, the former radius remains constant. Conversely, t_a remains constant up to 125 MW and then increases up to 175 MW.

Fig. 7(b) shows the I/I_c ratio at which the HTS tapes belonging to the different conductive layers operate. Fig. 7(c) presents the number of tapes used to wind each phase of the cable (adding those of their constitutive layers, if multiple).

As the active power increases, both the operating current and the former radius increase, and so does the number of HTS tapes per layer among which the current is distributed. However, the I/I_c ratio keeps rising, as the increase in the number of tapes is not proportional to the increase in current. In fact, once the upper limit for the former radius is reached at 125 MW, the number of tapes for the superconducting layers cannot vary significantly. As shown in (7), with $R_{i,j}$ fixed, $Tapes_{i,j}$ depends on the winding angle, which only allows a variation of around 5 tapes per layer in the interval of $\alpha_{i,j}$ selected by the user (from 0 to $\pm\,\pi/6$). Moreover, even $\alpha_{i,j}$ cannot vary freely, as it affects the inductances and consequently the current distribution between the three phases.

If the number of HTS tapes does not vary between 125 MW and 175 MW, their capital cost remains equal, as shown in Fig. 5(b). Increasing the I/I_c ratio causes a rapid growth of HTS AC losses, as shown in Fig. 6. However, this increase is limited by the safety criterion set by the user. By extending the curves referring to the first layer of phases 1 and 2 of Fig. 7(b) up to 200 MW, their I/I_c ratio could exceed the imposed limit value of 0.7. In order to comply with this constraint, the algorithm increases the number of superconducting layers for these two phases. As a result, passing from 175 MW to 200 MW, the number of tapes used to wind phases 1 and 2 almost doubles, as shown in Fig. 7(c). This explains the rapid increase in the corresponding capital cost contribution. The algorithm does not increase the number of layers of phase 3, as it is wound on a greater radius than that of the underlying phases and can work with a sufficient number of tapes in a single layer.

Finally, doubling the number of tapes, the I/I_c ratio for both layers of phase 1 and 2 drops when the active power is equal to 200 MW. This causes the reduction of the HTS AC losses and explains the trend shown in Fig. 6. However, if on the one hand the operating costs per kilometer are reduced by 1.3 M€ from 175 MW to 200 MW, on the other hand the capital costs increase by 3.2 M€ in the same power step, and therefore the total costs shown in Fig. 5(a) rise.

B.Impact of the HTS AC losses

As shown in Fig. 6, the main contributor to total losses and heat inputs into the cable is due to the AC losses generated in the superconductor. HTS AC losses have a significant impact on the optimized cable configuration, as they affect the operating and capital costs of the cooling stations, as well as the temperature increase of the coolant (and of the superconductor itself) in the cable segments. As described in Chapter III.A, in this study the AC losses are computed using Norris' analytic

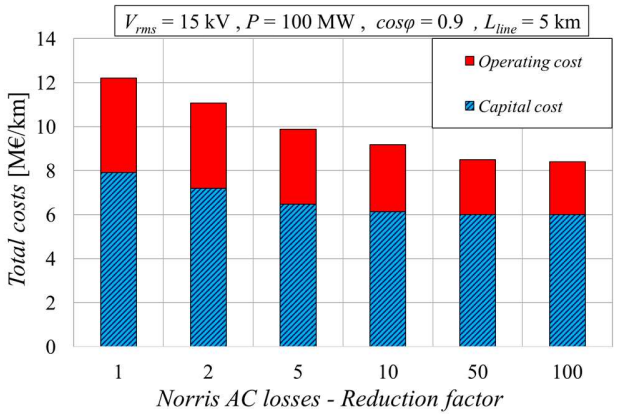

Fig. 8. Total costs per kilometer of cable varying the reduction factor applied to the Norris' formula for HTS AC losses. The case considered has V_{rms} = 15 kV, P = 100 MW, $cos\varphi$ = 0.9 and L_{line} = 5 km.

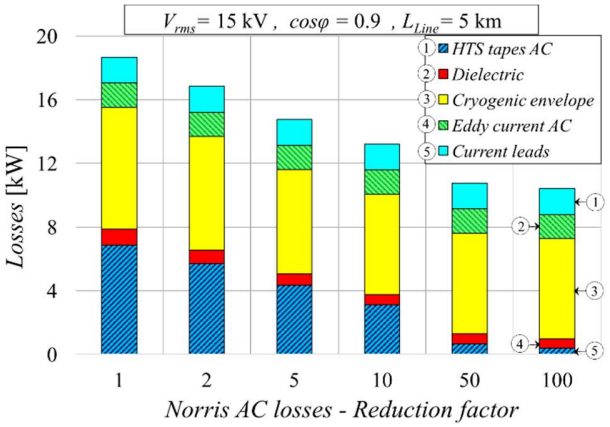

Fig. 9. Losses and heat inputs along the whole cable length varying the reduction factor applied to the Norris' formula for HTS AC losses. The case considered has V_{rms} = 15 kV, P = 100 MW, $cos\varphi$ = 0.9 and L_{line} = 5 km.

formula, considered as a conservative estimate and an upper limit compared to other formulae. Given the versatility of the proposed tool, it is interesting to study how the cost of the cable system varies if the losses generated in the superconductor are lower than those computed analytically. This allows to quantify the economic advantages that can be obtained by developing novel cable configurations or HTS tapes producing lower AC losses.

Fig. 8 shows the total costs per kilometer of cable obtained by applying different reduction factors to the Norris' formula (*i.e.* dividing the values found by the reduction factor). The case study considered is a 5 km long cable carrying 100 MW of active power to a load with $cos\varphi$ = 0.9, at a rated voltage equal to 15 kV.

Compared to the reference case (reduction factor equal to 1), the total costs are lowered by 9.3%, 19.1%, 28.8%, 30.3% and 31.1% when the losses are reduced by a factor of 2, 5, 10, 50 and 100, respectively. These results are significant, as they prove that, for the reference values presented in Chapter VII, even a significant change in the HTS AC losses estimate implemented in the model corresponds to a much smaller variation in the total cost of the system. Indeed, by reducing the losses by

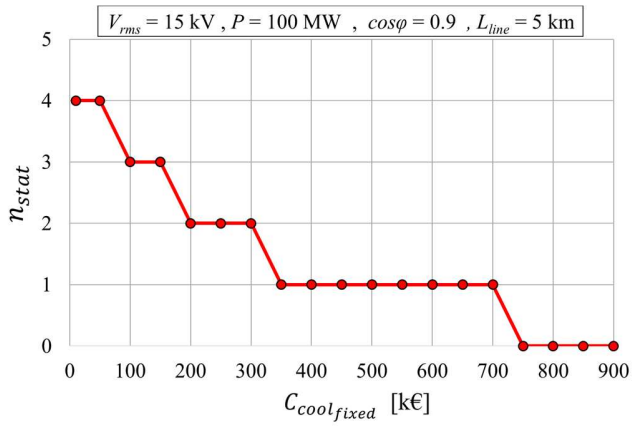

Fig. 10. Number of intermediate cooling stations varying the parameter $C_{cool_{fixed}}$. The case considered has V_{rms} = 15 kV, P = 100 MW, $cos\varphi$ = 0.9 and L_{line} = 5 km.

100 times compared to Norris' formula, the resulting total cost is reduced by only 31.1%. Therefore, even if the present analysis is performed using an analytical method for the computation of AC losses in the HTS tapes, which might not reach a high accuracy, the impact on the reliability of the results reported is limited.

As far as the capital costs are concerned, their reduction is mainly due to the possibility of using fewer tapes per phase (reducing the former radius), which makes them operate at I/I_c values closer to the imposed safety limit. Capital costs are lowered by 9.0%, 18.1%, 22.6%, 24.1% and 24.2% when the losses are reduced by a factor of 2, 5, 10, 50 and 100, respectively. Thus, capital costs get close to their asymptotic value for a reduction factor included between 10 to 50. Further reducing the AC loses generates small economic advantages, as the optimized former radius has already reached its lower limit and thus the minimum number of tapes per phase is fixed.

As for the operating costs, these are lowered by 9.9%, 20.9%, 29.1%, 41.6% and 43.7% when the losses are reduced by a factor of 2, 5, 10, 50 and 100, respectively. As shown in Fig. 9, with reduction factors greater than 50, HTS AC losses become almost negligible compared to the other loss contributions, and the cryogenic losses are prevalent.

C.Impact of the fixed costs of each cooling station

The parameter $C_{cool_{fixed}}$ is introduced in (32) to account for the fixed costs required for each cooling station besides the device cost. The presence of this parameter is important to obtain a realistic number for n_{stat}. In fact, without the term $C_{cool_{fixed}}$, the capital costs for each cooling station would only be dependent on the power to be extracted. It follows that, for the same total heat entering the cable, the optimization algorithm would impose n_{stat} to be equal to the upper boundary limit set by the user, as a greater number of cooling stations reduces d_{stat} and therefore the heat absorbed by the cryogenic fluid in each segment of the cable. In this way, the temperature rises in the segments are limited and the temperature and performance of the superconductor are more stable. By introducing fixed capital

TABLE VIII
OPTIMIZED CABLE CONFIGURATION FOR THE CASE OF CHAPTER VIII.D

Parameter	Unit	Value
$nl_1;\ nl_2\ ;\ nl_3$		1 , 1, 1
$\alpha_{1,1}\ ;\ \alpha_{2,1}\ ;\ \alpha_{3,1}$	°	-0.69 ; 0.41 ; -0.04
$Tapes_{1,1}; Tapes_{2,1}\ ;\ Tapes_{3,1}$		39 ; 42 ; 46
$\dot{m_{LN2}}$	kg/s	0.39
n_{stat}		2
d_{stat}	km	1.67
t_{an}	cm	1.0
R_f	cm	2.1
$R_{1,1}\ ;\ R_{2,1}\ ;\ R_{3,1}$	cm	2.45 ; 2.68 ; 2.90
$t_{ins_1}\ ;\ t_{ins_2}\ ;\ t_{ins_3}$	mm	2.5 ; 2.5 ; 2.5
R_n	cm	3.2
$R_{an_{int}}$	cm	3.5
$R_{an_{ext}}$	cm	4.5
$R_{cryo_{int}}$	cm	4.5
$R_{cryo_{ext}}$	cm	6.5
I_{rms}	kA	8.55
$\lvert\underline{I_{1,1}}\rvert\ ;\ \lvert\underline{I_{2,1}}\rvert\ ;\ \lvert\underline{I_{3,1}}\rvert$	kA	8.53 ; 8.55 ; 8. 57
Phase-shift of phase 1 , 2 , 3	°	-0.4 ; 120.1 ; 119.5
$I/I_{c_{1,1}}\ ;\ I/I_{c_{2,1}}\ ;\ I/I_{c_{3,1}}$		0.42 ; 0.39 ; 0.38
$V_{drop_{1,1}}\ ;\ V_{drop_{2,1}}\ ;\ V_{drop_{3,1}}$	% of V_{rms}	0.8 ; 0.5 ; 0.1
Distance between adjacent tapes in the same layer	% of w_{HTS}	0.8 ; 0.3 ; 0.9
ΔP_f	bar	0.31
ΔP_{ann}	bar	5.0
ΔT_f	K	0.8
ΔT_{ann}	K	2.5
$T_{HTS_{left}}\ ;\ T_{HTS_{right}}$	K	69.3 ; 68.4
$L_{lay_{1,1}} + L_{lay_{2,1}} + L_{lay_{3,1}}$	km	635.0
C_{tot}	M€	61.0
C_{cap} *for the whole cable system*	M€	39.6
C_{op} *for the whole cable system*	M€	21.4
C_{HTS}	M€	22.2
C_{cool}	M€	17.0
C_{cryo}	M€	1.1
C_{vac}	M€	0.26
C_{ter}	M€	0.3
C_{cab}	M€	12.5
C_{lay}	M€	0.1
C_{ins}	k€	52.0
C_{LN2}	k€	20.0
C_{man}	k€	49.0
C_{dis}	k€	96.1
$Q_{AC\ TOT} = Q_{AC} \cdot L_{line}$	kW	6.9
$Q_{ins\ TOT} = Q_{ins} \cdot L_{line}$	kW	1.0
$Q_{ed\ TOT} = Q_{ed} \cdot L_{line}$	kW	1.5
$Q_{cryo\ TOT} = Q_{cryo} \cdot L_{line}$	kW	7.6
Q_{cl}	kW	1.6

costs due to the installation of a cooling station, the algorithm must balance this cost contribution with the reduction in tape performance (which affects other cost contributions).

Fig. 10 shows how the number of intermediate stations varies by setting different $C_{cool_{fixed}}$ values as computation inputs. In the case study considered (V_{rms} = 15 kV, P = 100 MW, $cos\varphi$ = 0.9 and L_{line} = 5 km), when $C_{cool_{fixed}}$ is lower than 50 k€, the tool returns a number of stations equal to the upper boundary imposed in this study (corresponding to the cable length, expressed in kilometers, minus 1). As their capital cost increases, the number of stations is reduced. When $C_{cool_{fixed}}$ is larger than 700 k€, it is not convenient to use intermediate cooling stations. The value of $C_{cool_{fixed}}$ shown in Table VI (200 k€,) is selected according to this analysis.

D.Impact of the fixed costs of each cooling station

Finally, it is useful to show a complete cable system configuration resulting from the optimization process. The case of a 5 km long cable carrying 100 MW of active power to a load with $cos\varphi$ = 0.9, at a voltage level equal to 15 kV is selected.
Table VIII shows the values of the system variables, the main resulting geometric and electrical parameters of the cable and the verification of compliance with the constraints.

IX.CONCLUSIONS

This work proposes a model to determine the optimal configuration of an AC power transport cable wound with HTS tapes, that minimizes the total cost of the system. The tool developed allows the user to freely select the operating conditions for a generic electric line, a feature rarely present in the estimates for the cost and/or cable configuration available in the literature.
The constrained multi-variable optimization adopted is based on a genetic algorithm implemented in MATLAB.

Some simplifications are adopted to ease the identification of the parametric equations of the model and to allow a fast resolution, thus limiting the number of cases to be analyzed. The main assumptions used in this work are conveniently reported here:

- the so-called *concentric cable* configuration is investigated;
- the so-called *both-sided cooling option* is considered, having two counter-flows of coolant flowing in the former and in the annular gap;
- the system variables for the genetic algorithm are the radius of the former, the thickness of the annular gap, the number of superconducting layers per phase and the corresponding winding angle, the number of intermediate cooling stations and the nitrogen mass flow rate. The remaining cable parameters are derived from the system variables or are user-defined;
- the system is modular: the configuration of each cable segment included between adjacent cooling stations is the same;
- a single temperature is considered for all the HTS tapes at each longitudinal position along the cable length;
- the temperature increase and the pressure drop of the coolant are assumed linear within each cable segment. Moreover, the incompressible fluid assumption is adopted;

- the losses are shared equally between the two flows, with the exception of the heat entering the cryostat, which is absorbed by the nitrogen in the annular gap only;
- the impact of the equivalent longitudinal resistance of the superconducting layers on the current distribution is negligible;

Future model developments may allow to remove some of these simplifications thus extending the field of applicability of the model.

The model is based on analytic equations for the calculation of the heat entering the system, for the computation of the dielectric thickness and for the cost estimation. In particular, the cost function to be minimized includes several contributions rarely reported in full in the literature. Different electrical constraints are applied to the algorithm, related to the current distribution between tapes, layers and phases, as well as thermo-fluidynamic constraints related to pressure drops and temperature increases in the coolant. An extensive bibliographic work is carried out to identify the numerous model parameters and indexes and report the corresponding references.

The effectiveness and versatility of the developed tool is proved through explicative parametric analyses. In particular, the trends of the system costs are shown by varying the active power of the line (at a fixed voltage level in the medium voltage range), the length of the line and the power factor of the load connected to the cable. As the transmitted power increases, the total cost of the system rises. However, the increases in capital and operating costs do not vary linearly with power. In fact, when increasing the power, the former radius reaches its user defined upper limit, which consequently binds the radial dimensions of the overlying conductive layers and the number of tapes. By further increasing the power, the I/I_c ratio grows (increasing the HTS AC losses and the operating costs) and approaches the safety limit imposed as a constraint. To comply with this constraint, the algorithm adds one or more conductive layers per phase, increasing the capital costs related to the HTS tape but reducing the HTS AC losses.

A specific analysis is carried out to investigate the impact of a possible reduction of HTS AC losses (the main loss contribution together with the heat inputs from the cryostat) with respect to those computed with the Norris' analytic formula. In particular, it is shown that with a loss reduction up to 50 times with respect to Norris' formula results, the economic advantage is maximized; further reductions do not significantly affect the system costs.

Moreover, the computations allow a better understanding of the role of the parameter $C_{cool_{fixed}}$, introduced in the model to account for the fixed costs related to the cooling stations. If this term is set to be low, the optimized number of intermediate cooling stations tends to correspond to the maximum value set by the user. As this cost increases, the economic convenience of introducing many intermediate stations is reduced and their number is limited.

The approach and methodology described in this work can conveniently be adapted to several other HTS cable configurations. The design tool developed is flexible enough to be applied to parametric analyses over a wide range of user defined parameters. It can either be adopted to study the retrofitting of existing conventional transmission lines or, with slight modifications, to the sizing of new superconducting lines.

REFERENCES

[1] R. L. Garwin and J. Matisoo, "Superconducting lines for the transmission of large amounts of electric power over great distances," Proceedings of the IEEE, vol. 55, no. 4, 1967.

[2] E. B. Forsyth and R. A. Thomas, "Performance summary of the Brookhaven superconducting power transmission system," Cryogenics, vol. 26, 1986.

[3] A. P. Malozemoff et al., "High-temperature superconducting (HTS) AC cables for power grid applications," Superconductors in the Power Grid Materials and Applications, Woodhead Publishing Series in Energy, pp. 133-188, 2015.

[4] F. Schmidt and A. Allais, "Superconducting cables for power transmission applications - a review," Workshop on accelerator magnet superconductors (WAMS) Proceedings, p. 352, Archamps - France, Mar. 2004.

[5] N. Kelley et al., "Application of HTS wire and cables to power transmission state of the art and opportunities," IEEE Power Engineering Society Winter Meeting. Conference Proceedings, 2001.

[6] S. Honjo et al., "Electric properties of a 66 kV 3-core superconducting power cable system," IEEE Trans. on Appl. Supercond, vol. 13, no. 2, 2003.

[7] D. W. Kim et al., "Development of the 22.9-kV class HTS power cable in LG cable," IEEE Trans. on Appl. Supercond., vol. 15, no. 2, 2005.

[8] T. Takahashi et al., "Demonstration and verification tests of 500 m long HTS power cable," IEEE Trans. on Appl. Supercond., vol. 15, no. 2, 2005.

[9] J. F. Maguire et al., "Progress and status of a 2G HTS power cable to be installed in the Long Island Power Authority (LIPA) grid," IEEE Trans. on Appl. Supercond., vol. 21, no. 3, pp. 961–966, 2011.

[10] K. Sim et al., "DC critical current and AC loss measurement of the 100 m 22.9 kV/50 MVA HTS cable," Physica C, vol. 468, pp. 2018–2022, 2008.

[11] R. Soika et al., "ENDESA supercable, a 3.2 kA, 138 MVA, medium voltage superconducting power cable," IEEE Trans. on Appl. Supercond., vol. 21, no. 3, pp. 972–975, 2011.

[12] H. Yumura et al., "Update of Yokohama HTS cable project," IEEE Trans. on Appl. Supercond, vol. 23, no. 3, 2013.

[13] S. Lee et al., "Modeling of a 22.9 kV 50 MVA superconducting power cable based on PSCAD/EMTDC for application to the Icheon substation in Korea," Physica C: Superconductivity and Its Applications, vol. 471, no. 21, pp. 1283–1289, 2011.

[14] O. Maruyama et al., "Development of 66 kV and 275 kV class REBCO HTS power cables," IEEE Trans. on Appl. Supercond., vol. 23, no. 3, 2013.

[15] M. Stemmle et al., "AmpaCity e installation of advanced superconducting 10 kV system in city center replaces conventional 110 kV cables," IEEE International Conference on Applied Superconductivity and Electromagnetic Devices, pp. 323–3265, 2013.

[16] E. P. Volkov et al., "First Russian long length HTS power cable," Physica C, vol. 482, pp. 87–91, 2012.

[17] J. Maguire et al., "Status and progress of a fault current limiting HTS cable to be installed in the Con Edison grid," Advances in Cryogenic Engineering, vol. 55A, pp. 445–452, 2009.

[18] M. Nassi et al., "Qualification results of a 50 m e 115 kV warm dielectric cable system," IEEE Trans. on Appl. Supercond., vol. 11, no. 1, pp. 2355–2358, 2001.

[19] O. Tonnesen et al., "Operation experiences with a 30 kV/100MVA high temperature superconducting cable system," Supercond. Sci. and Technol., vol. 17, 2004.

[20] Y. Xin et al., "Introduction of China's first live grid installed HTS power cable system," IEEE Trans. on Appl. Supercond., vol. 15, no. 2, pp. 1814–1817, 2005.

[21] L. Xiao et al., "Development of HTS AC power transmission cables," IEEE Trans. on Appl. Supercond., vol. 17, no. 2, pp. 1652–1655, 2007.

[22] D. Politano et al., "Technical and Economical Assessment of HTS Cables," IEEE Trans. on Appl. Supercond., vol. 11, no. 1, pp. 2477–2480, 2001.

[23] S. Fukui et al., "Numerical study on AC loss minimization of multi-layer tri-axial HTS cable for 3-phase AC power transmission," IEEE Trans. on Appl. Supercond., vol. 17, no. 2, pp. 1700–1703, 2007.

[24] W. T. B. de Sousa et al., "An open-source 2D finite difference based transient electro-thermal simulation model for three-phase concentric superconducting power cables," Supercond. Sci. Technol, vol. 34, 2021.

[25] MATLAB. Version 2020a, The Math Works Inc., Natick, Massachusetts, United States, 2020.

[26] D. Kottonau et al., "Design Comparisons of Concentric Three-Phase HTS Cables," IEEE Trans. On Appl. Supercond., vol. 29, no. 6, Sept. 2019.

[27] W. T. Norris, "Calculation of hysteresis losses in hard superconductors carrying AC isolated conductors and edges of thin sheets," J. Phys. Appl. Phys., vol. 3, no. 4, pp. 489–507, Apr. 1970.

[28] G. Vellego and P. Metra, "An analysis of the transport losses measured on HTSC single-phase conductor prototypes," Supercond. Sci. Technol., vol. 8, pp. 476–483, 1995.

[29] M. Daumling, "Ac loss in two ac carrying superconducting concentric tubes—the duoblock model," Phys. C, vol. 403, pp. 57–59, 2004.

[30] J. R. Clem and A. P. Malozemoff, "Flux transfer losses in helically wound superconducting power cables,". Supercond. Sci. Technol., vol. 26, no. 085008. 2010.

[31] A. P. Malozemoff et al., "Tape-Width Dependence of AC Losses in HTS Cables," IEEE Trans. on Appl. Supercond., vol. 19, no. 3, 2009.

[32] V. E. Sytnikov et al., "The AC Loss Analysis in the 5 m HTS Power Cables," IEEE Trans. on Appl. Supercond., vol. 19, no. 3, 2009.

[33] N. Amemiya et al., "AC Loss Reduction of Superconducting Power Transmission Cables Composed of Coated Conductors," IEEE Trans. on Appl. Supercond., vol. 17, no. 2, 2017.

[34] D. Kottonau et al., "Evaluation of the Use of Superconducting 380 kV Cable," KIT Scientific publishing, 2020.

[35] L. Trevisani, "Design and simulation of a large scale energy storage and power transmission system for remote renewable energy sources exploitation," Ph.D. Dissertation, University of Bologna, Italy, 2006.

[36] J. A. Demko, "8 - High-temperature superconducting cable cooling systems for power grid applications," Superconductors in the Power Grid, Woodhead Publishing Series in Energy, pp. 261-280, 2015.

[37] M. J. Gouge et al., "Vacuum-insulated, flexible cryostat for long HTS cables requirements: Status and prospects", AIP Conference Proceedings, Vol. 985, No. 1, pp. 1343-1350, 2008.

[38] F. Schmidt et al., "Operation Experience and further Development of a High-Temperature Superconducting Power Cable in the Long Island Power Authority Grid", Physics Procedia, vol. 36, Pages 1137-1144, 2012.

[39] M. J. Gouge et al.," Tests of tri-axial HTS cables," IEEE Trans Appl Supercond, vol. 15, no. 2, pp. 1827–1830, 2005.

[40] T. Masuda et al., "Development of a 100m, 3-core 114MVA HTSC cable system," Phys C, vol. 372–376, no. 3, pp. 1580–1584, 2002.

[41] S. Mukoyama et al., "Demonstration and verification tests of a 500m HTS cable in the super-ACE project," Phys C, vol. 426–431, pp. 1365–1373 2005.

[42] J. A. Demko et al., "Cryostat vacuum thermal considerations for HTS power transmission cable systems," IEEE Trans Appl Supercond, vol. 13, no. 2, pp. 1930–1933, 2003.

[43] J. Choi et al. "A Study on Insulation Characteristics of Laminated Polypropylene Paper for an HTS Cable," IEEE Trans. On Appl. Supercond., vol. 20, no. 3, 2010.

[44] D. S. Kwag et al. "A Study on the Composite Dielectric Properties for an HTS Cable," IEEE Trans. On Appl. Supercond., vol. 15, no. 2, 2005.

[45] W. Pi et al., "Insulation Design and Simulation for Three-Phase Concentric High-Temperature Superconducting Cable Under 10-kV Power System", IEEE Trans. On Appl. Supercond., vol. 29, 2019.

[46] A. Morandi, "HTS dc transmission and distribution: concepts, applications and benefits," Supercond. Sci. Technol., vol. 28, p. 123001, 2015.

[47] N. Hayakawa, "Insulation technologies for HTS apparatus," ESAS Summer School on HTS Technology for Sustainable Energy and Transport Systems, Bologna-Italy, Jun. 2016.

[48] T. Nguyen et al. "A Simplified Model of Coaxial, Multilayer High-Temperature Superconducting Power Cables with Cu Formers for Transient Studies," Energies, vol. 12, 2019.

[49] S. Kim et al., "Effect of winding direction on four-layer HTS power transmission cable," Cryogenics, vol. 43, pp. 629–635, 2003.

[50] J. Zhu et al., "Inductance and Current Distribution Analysis of a Prototype HTS Cable," J. Phys.: Conf. Ser., vol. 507, p. 022047, 2014.

[51] C. Colebrook, "Turbulent Flow in Pipes with Particular Reference to the Transition Region between the Smooth and Rough Pipe Laws," J. Institution of Civil Engineers, vol. 11, pp. 133-156, 1939.

[52] S. E. Haaland, "Simple and Explicit formulas for friction factor in turbulent pipe flow," J. Fluid Eng, vol. 105, no. 1, 1983.

[53] S. Kloppel et al., "Thermo-hydraulic and economic aspects of long-length high-power MgB2 superconducting cables," Cryogenics, vol. 113, p. 103211, Oct. 2020.

[54] K. Takeuchi et al., "Model for electromagnetic field analysis of superconducting power transmission cable comprising spiraled coated conductors," Supercond. Sci. and Technol., vol. 24, no. 085014, 2011.

[55] V. A. Altov et al., "Optimization of Three- and Single-Phase AC HTS Cables Design by Numerical Simulation," IEEE Trans. on Appl. Supercond., vol. 27, no. 4, p. 4801606, Jun. 2017.

[56] H. Thomas et al., "Superconducting transmission lines – Sustainable electric energy transfer with higher public acceptance?," Renewable and Sustainable Energy Reviews, vol. 55, pp. 59–72, Nov. 2016.

[57] L. Ren et al., "Techno-Economic Feasibility Study on HTS Power Cables," IEEE Trans. On Appl. Supercond., vol. 19, no. 3, pp. 1774–1777, Jun. 2009.

[58] M. Elsherif et al., "Investigating the potential impact of superconducting distribution networks," p. 0816, 22nd International Conference on Electricity Distribution, Stockholm, Jun. 2013.

[59] W. Yuan et al., "Economic Feasibility Study of using High Temperature Superconducting cables in UK's Electrical Distribution Networks," IEEE Trans. On Appl. Supercond., vol. 28, no. 4, p. 5401505, Jan. 2018.

[60] P. C. Ferran, "Economical study of electric power transmission with superconducting lines for HVDC systems," Ph.D Thesis, Escola Tècnica Superior d'Enginyeria Industrial de Barcelona, Spain, Jun. 2021.

[61] Z. Yu et al., "Feasibility and Economical Analysis of the Superconducting Cable and Hydrogen Hybrid Transmission Gallery," Proceedings of 2020 IEEE International Conference on Applied Superconductivity and Electromagnetic Devices Tianjin, China, Oct. 2020

[62] S. H. Venuturumilli et al., "Superconducting Cables-Network Feasibility Study Work Package 3", 2017. https://www.westernpower.co.uk/downloads-view-reciteme/2152

[63] R. Guarino et al., "Technical and economic feasibility study of high-current HTS bus bars for fusion reactors," Physica C: Superconductivity and its applications, vol. 592, n. 1353996, 2022.

[64] https://ec.europa.eu/eurostat/databrowser/view/ten00117

[65] CEI (Comitato Elettrotecnico Italiano) norm 64-8 for electrical systems users – Chapter 525: Voltage drop in user systems, 8th Ed., ISBN: 978-88-432-0119-8, 2021.

[66] T. Takahashi et al., "Dielectric Properties of 500 m Long HTS Power Cable", IEEE Trans. On Appl. Supercond., vol. 15, 2005.

[67] H. Suzuki et al., "Electrical insulation characteristics of liquid nitrogen impregnated laminated paper insulated cable", IEEE Transactions on Power Delivery, vol. 7, 1992.

[68] G. Wypych, "HDPE high density polyethylene, Handbook of Polymers," Elsevier, ISBN 9781895198478, pp. 150-156, 2012.

[69] M. Gouge, "Flexible Cryostats for Superconducting Cables: Reliability and Lifetime Issues", Wire Development Workshop, Session VII, February 2006.

[70] F. Herzog, "Cooling unit for the AmpaCity project – One year successful operation", Cryogenics, vol. 80, 2016.

[71] C. Lee et al., "Economic Evaluation of 23 kV Tri-Axial HTS Cable Application to Power Systems," IEEE Trans. On Appl. Supercond., vol. 25, no.5, p. 5402507, 2019.

[72] Roy Zuijderduin, "Integration of High-Tc Superconducting Cables in the Dutch Power Grid of the Future," Ph.D. Thesis, Delft University of Technology, The Netherlands, 2016.

[73] N. C. Allen et al., "Numerical and experimental investigation of the electromechanical behaviour of rebco tapes," IOP Conf. Ser.: Mater. Sci. Eng., vol. 102, p. 012025, 2015.

[74] S. Wimbush and N. Strickland, "Critical current characterisation of SuNAM SAN04200 2G HTS superconducting wire," Figshare Dataset, https://doi.org/10.6084/m9.figshare.5182354.v1, 2017.